

More on the operator space entanglement (*OSE*): Rényi *OSE*, revivals, and integrability breaking.

Vincenzo Alba

¹Dipartimento di Fisica dell'Università di Pisa and INFN, Sezione di Pisa, I-56127 Pisa, Italy

E-mail: vincenzo.alba@unipi.it

Abstract.

We investigate the dynamics of the Rényi Operator Space Entanglement (*OSE*) entropies S_n across several one-dimensional integrable and chaotic models. As a paradigmatic integrable system, we first consider the so-called rule 54 chain. Our numerical results reveal that the Rényi *OSE* entropies of diagonal operators with nonzero trace saturate at long times, in contrast with the behavior of von Neumann entropy. Oppositely, the Rényi entropies of traceless operators exhibit logarithmic growth with time, with the prefactor of this growth depending in a nontrivial manner on n . Notably, at long times, the complete operator entanglement spectrum (*ES*) of an operator can be reconstructed from the spectrum of its traceless part. We observe a similar pattern in the *XXZ* chain, suggesting universal behavior. Additionally, we consider dynamics in nonintegrable deformations of the *XXZ* chain. Finite-time corrections do not allow to access the long-time behavior of the von Neumann entropy. On the other hand, for $n > 1$ the growth of the entropies is milder, and it is compatible with a sublinear growth, at least for operators associated with global conserved quantities. Finally, we show that in finite-size integrable systems, S_n exhibit strong revivals, which are washed out when integrability is broken.

1. Introduction

The entanglement growth in typical out-of-equilibrium dynamics [1, 2, 3, 4, 5, 6] significantly hinders the simulation of out-of-equilibrium quantum many-body systems with state-of-the-art numerical methods, such as the time-dependent Density Matrix Renormalization Group [7, 8] (*tDMRG*). Early research into *tDMRG* suggested that instead of simulating the dynamics of the full quantum state, it could be convenient to focus on the Heisenberg dynamics of operators. The Heisenberg evolution of an operator $\hat{\mathcal{O}}$ is expressed as

$$\hat{\mathcal{O}}(t) = \hat{U}^\dagger(t)\hat{\mathcal{O}}(0)\hat{U}(t), \quad \hat{U}(t) := e^{-iHt/\hbar}, \quad (1)$$

with H the Hamiltonian of the system. Here we restrict ourselves to one-dimensional lattice models (spin chains), considering a generic local operator $\hat{\mathcal{O}}$ that acts nontrivially only at the center of the chain, and is the identity elsewhere (see Fig. 1). It is important to quantify the complexity of the operator growth, particularly by constructing the time-dependent Matrix Product Operator [8] (*MPO*) of $\hat{\mathcal{O}}$.

The construction of *MPOs* is illustrated in Fig. 1 (a). Let us consider a generic operator \mathcal{O} living on a system of L sites. We focus on spin-1/2 systems. The operator \mathcal{O} is represented as a $2^L \times 2^L$ matrix (see the box in Fig. 1 (a)) in the standard computational basis $|\sigma_1, \sigma_2, \dots, \sigma_L\rangle$, with $\sigma_j = \uparrow, \downarrow$. Let us bipartite the system as $A \cup B$ (see Fig. 1). It is always possible to perform a Schmidt decomposition of $\hat{\mathcal{O}}$ as

$$\frac{\hat{\mathcal{O}}(t)}{\sqrt{\text{Tr}(\hat{\mathcal{O}}^\dagger \hat{\mathcal{O}})}} = \sum_i \sqrt{\lambda_i} \hat{\mathcal{O}}_{A,i} \otimes \hat{\mathcal{O}}_{B,i}, \quad (2)$$

where $\hat{\mathcal{O}}_{A/B,i}$ are two orthonormal sets of operators with support in A and B , satisfying $\text{Tr}(\hat{\mathcal{O}}_{A/B,i}^\dagger \hat{\mathcal{O}}_{A/B,j}) = \delta_{ij}$. In (2) $\sqrt{\lambda_i}$ are the so-called Schmidt values. The decomposition in (2) (see Fig. 1) is exact. By keeping only the largest χ Schmidt numbers, one obtains a truncated representation of $\hat{\mathcal{O}}$. Moreover, by iterating the Schmidt decomposition within the two regions A, B , keeping at each step the largest χ Schmidt values, one arrives at a compressed *MPO* representation of $\hat{\mathcal{O}}$. In contrast with the original representation of the operator, which depends on 2^{2L} complex numbers, the *MPO* is determined by $d^2 \chi L$ numbers, where $d = 2$ is the dimension of the local Hilbert space. Here we consider operators that at $t = 0$ act nontrivially only at the center of the chain, and are the identity elsewhere. The *MPO* of such operators at $t = 0$ is exact with bond dimension $\chi = 1$. Understanding the growth of the bond dimension χ as a function of time is crucial to quantify the effectiveness of the *MPO* decomposition.

Quite generically, at $t > 0$ a double lightcone spreads from the center of the chain (see Fig. 1 (b)), as the operator support, i.e., the sites of the chain where the operator acts nontrivially, expands with time. This is typically accompanied by the growth of χ of the operators that live within the lightcone. Based on exact results in noninteracting systems, Ref. [9] conjectured that there is a significant difference between integrable and nonintegrable dynamics: In integrable systems the bond dimension necessary for a fixed

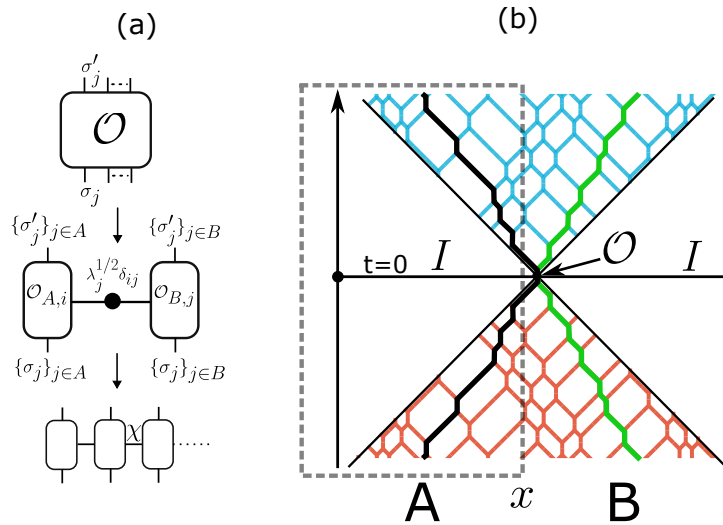


Figure 1. Setup considered in this work. Panel (a) shows the Matrix Product Operator (MPO) representation of a generic operator \mathcal{O} . \mathcal{O} is represented as a box, the legs being the row and column indices σ_j and σ'_j . Here we restrict ourselves to spin-1/2 systems with $\sigma_j, \sigma'_j = \uparrow, \downarrow$. \mathcal{O} is represented as a $2^L \times 2^L$ matrix, with L the total number of sites. By dividing the system in two complementary regions A and B , one can always perform a Schmidt decomposition of the operator (cf. (2)) in terms of two orthonormal bases $\mathcal{O}_{A,i}$ and $\mathcal{O}_{B,j}$ for A, B and the singular values $\sqrt{\lambda_j}$. By iterating the Schmidt decomposition within A and B and keeping at each step the largest χ (bond dimension) singular values only, one obtains a compressed MPO representation for \mathcal{O} . (b) We study the Heisenberg evolution $\hat{\mathcal{O}}(t) = e^{iHt/h} \hat{\mathcal{O}} e^{-iHt/h}$ of a local operator $\hat{\mathcal{O}}$ acting nontrivially at the center of a one dimensional system. Away from the center the operator acts as the identity. As time progresses, the support of the operator spreads, forming a double lightcone. For diagonal operators, the upper and lower parts of the lightcone coincide. We study the dynamics of the Rényi Operator Space Entanglement (OSE) entropies $S_n(\hat{\mathcal{O}})$ ($n \in \mathbb{N}$) of region A , starting at position x . Here we fix $x = 0$, meaning that A is the half chain starting from the operator insertion. In the rule 54 chain the operator spreading is understood in terms of interacting left and right movers (solitons).

fidelity approximation of a local operator grows only polynomially with time, whereas nonintegrable Hamiltonians lead to an exponential growth of χ .

The operator space entanglement (OSE) entropies [10] $S_n(\hat{\mathcal{O}})$ provide the means to quantify the growth of χ with time, and to address these issues. In the following we mostly consider the situation with A and B being the two halves of the chain. We also fix $x = 0$ (see Fig. 1), placing the boundary between A and B at the operator insertion. The Rényi OSE entropies S_n and the von Neumann one S_1 are defined as

$$S_n(\hat{\mathcal{O}}) = \frac{1}{1-n} \ln \left(\sum_i \lambda_i^n \right), \quad S_1 = - \sum_i \lambda_i \ln(\lambda_i). \quad (3)$$

Now, according to the conjecture in Ref. [9], integrable dynamics lead to at most a logarithmic growth of S_n with time, whereas nonintegrable ones are expected to give linear growth of S_n . This scenario was first verified in noninteracting models [11, 12, 13].

Recently, it has been shown [14, 15] that the von Neumann *OSE* entropy can grow at most logarithmically with time in the rule 54 chain [16, 17], which has been studied intensively [18, 19, 20, 21, 22, 23] as a toy model of interacting integrable systems. Precisely, based on previous results in Ref. [24], Ref. [14] provided an algorithm to construct the *MPO* for a generic local operator $\hat{O}(t)$. Crucially, the bond dimension χ grows as t^2 , which implies that S_n can grow only logarithmically with time. Moreover, Ref. [14] numerically showed that a similar logarithmic bound holds in Bethe ansatz solvable systems, such as the spin-1/2 Heisenberg *XXZ* chain. The linear-growth scenario for nonintegrable dynamics is supported by simulations in random unitary circuits, for which a so-called “membrane” picture for entanglement spreading applies [25, 26, 27, 28, 29]. Exact results in solvable chaotic quantum circuits [30, 31, 32, 33, 34, 35, 36] are also in agreement with the membrane picture.

Several open questions remain to be investigated. For instance, the mechanism underlying the growth of the *OSE* has not been clarified yet. While Ref. [14] showed logarithmic growth for the *OSE* entropies in integrable systems, the prefactor of the logarithmic growth is not understood, except for some simple operators [15]. More importantly, the relationship between transport properties and operator spreading, if any, is yet to be unveiled. Still, it has been argued in Ref. [15] that the growth of the *OSE* of some simple operators reflects the diffusive fluctuations of the operator front [37]. Furthermore, while a lot of attention has been devoted to the von Neumann *OSE* entropy, much less is known about the Rényi entropies, or the operator entanglement spectrum (*ES*) formed by the squared Schmidt values $\{\lambda_i\}$ (cf. (2)). Clearly, it is of utmost importance to understand the scaling of *OSE* in nonintegrable Hamiltonians. Unfortunately, this is a daunting task from the numerical perspective, as *tDMRG* methods rely on the mild growth of the bond dimension with time. Interestingly, it has been suggested [38] (see also Section 3) that even in nonintegrable systems the *OSE* entropies of operators linked with global conservation laws could exhibit logarithmic growth with time, in contrast with the membrane-picture scenario.

Here we address some of these open questions focusing on diagonal operators. We first consider the dynamics of the Rényi entropies in the rule 54 chain. We show that there is a crucial distinction to be made between traceless operators and operators with nonzero trace. Precisely, S_n grow logarithmically for any n for traceless diagonal operators. The prefactor of the logarithmic growth depends on n in a nontrivial manner, and it is different from that governing the logarithmic growth of operators in noninteracting systems [13], which can be obtained with Conformal Field Theory (*CFT*) techniques. We also investigate the distribution of the operator entanglement spectrum levels, which shows marked differences with that obtained in Conformal Field Theories [39]. Oppositely, the entropies S_n of operators with nonzero trace grow logarithmically with time only for $n = 1$, in agreement with previous results [14, 15]. For $n \neq 1$, S_n saturate at long times, the saturation values being fully determined by the trace of the operator. Interestingly, we show that the complete entanglement spectrum of an operator can be determined from the spectrum of its traceless part. We should

mention that while the same results were presented as an approximation in Ref. [26], here we provide evidence that they become asymptotically exact in the long time limit. To address the universality of our results, we consider the spin-1/2 *XXZ* chain, which is a paradigmatic interacting integrable system. The same scenario uncovered for the rule 54 chain applies: Both the Rényi and the von Neumann entropies of traceless operators grow logarithmically with time for any n . Interestingly, within the accuracy of our *tDMRG* simulations, the dependence on n of the prefactors of the logarithmic growth is the same as in the rule 54 chain, suggesting the same underlying mechanism for operator spreading in the two models. The Rényi *OSE* entropies of operators with nonzero trace saturate at long time.

Next we consider the effects of breaking integrability, focusing on the *XXZ* chain with next-nearest-neighbor interactions. First, we observe that S_n exhibit strong finite-time corrections. This makes challenging to determine the asymptotic behavior of the von Neumann entropy at long times. On the other hand, our numerical results for S_n with $n > 1$ are consistent with a quite mild growth in agreement with the bound of Ref. [38]. Finally, we investigate revival effects in finite-size chains. We show that for dynamics in the *XXZ* chain, which is integrable, the entropies exhibit revivals at times $t \approx L/2$. Revivals correspond to localized quasiparticles originated at the center of the chain that re-enter subsystem A after bouncing back at the boundary of the system. Interestingly, in the presence of integrability-breaking interactions, the revivals are washed out, which reflects the absence of well-defined quasiparticles.

The manuscript is organized as follows. In Section 2 we introduce the rule 54 chain (in Section 2.1) and the deformed *XXZ* chain (in Section 2.1). In particular, in Section 2.1 we discuss some general results for operator spreading in integrable systems. In Section 3 we review exact results for the *OSE* entropies. Specifically, in Section 3.1 we focus on Ref. [38], which provided an exact bound between Rényi entropies of an operator \hat{O} and its Infinite Temperature Auto Correlator (*ITAC*) $\langle \hat{O}(t)\hat{O}(0) \rangle_{T=\infty}$, with $\langle \cdot \rangle_{T=\infty}$ denoting the average over the infinite-temperature ensemble. In Section 3.2, following Ref. [26], we discuss the relationship between the operator entanglement spectrum of traceless operators and that of operators with nonzero trace. In Section 3.3 we discuss the results of Ref. [15]. In Section 4 we present numerical *tDMRG* data for the dynamics of diagonal operators in the rule 54 chain. Precisely, in Section 4.1 we show that for operators with nonzero trace only the von Neumann entropy grows logarithmically, whereas the Rényi entropies saturate at long times. In Section 4.2 we show that the Rényi entropies of traceless operators grow logarithmically. The dynamics of the operator entanglement spectrum is discussed in Section 4.3. In Section 5 we focus on the *XXZ* chain. In Section 5.1 we compare the behavior of the Rényi entropies of traceless and operators with nonzero trace, showing that the same scenario discussed for the rule 54 chain in Section 4 applies. Section 5.2 is devoted to the effects of integrability breaking. In Section 5.3 we discuss revivals in finite-size integrable and nonintegrable systems. We conclude in Section 6.

2. Models & setup: Operator spreading in the rule 54 chain and the XXZ chain

Here we introduce the two models that we will consider in this work, namely the so-called rule 54 chain and a nonintegrable deformation of the XXZ chain. Specifically, in Section 2.1 we discuss extensively the operator spreading in the rule 54 chain, as it is paradigmatic of generic integrable systems. In Section 2.2 we introduce the spin-1/2 Heisenberg XXZ chain with next-to-nearest-neighbor interactions, which allows to investigate both integrable and nonintegrable dynamics.

2.1. Rule 54 chain

The Hilbert space of the rule 54 chain [16] is that of a system of classical bits $s_x = 0, 1$. The system lives on a chain of L sites. The dynamics is generated by a three-site unitary gate U_x acting as

$$U_x = |s_{x-1}, s'_x, s_{x+1}\rangle\langle s_{x-1}s_x, s_{x+1}|, \quad (4)$$

where $s'_x = s_x + s_{x-1} + s_{x+1} - s_{x-1}s_{x+1} \bmod 2$. Precisely, one has

$$U_x = |101\rangle\langle 111| + |100\rangle\langle 110| + |111\rangle\langle 101| + |110\rangle\langle 100| \\ + |001\rangle\langle 011| + |010\rangle\langle 010| + |011\rangle\langle 001| + |000\rangle\langle 000|. \quad (5)$$

As it is clear from (4) and (5), U_x flips the bit at position x if at least one of its neighboring bits at $x-1$ and $x+1$ is in the state 1. Any bit configuration is evolved by applying U_x in a “brick-wall” fashion as $U = \prod_{\text{even } x} \prod_{\text{odd } x} U_x$. Time is discrete in units of 1. Clearly, Eq. (4) maps classical bit strings into classical bit strings. The rule 54 chain possesses well-defined quasiparticles (see Fig. 1), which is the key property of generic integrable systems. Quasiparticles are emergent left/right moving solitons. Precisely, solitons are formed by pairs of adjacent bits that are in the 1 state. Depending on the parity of the site of the leftmost 1 of the pair, they are left or right moving solitons [24]. The velocity of the solitons is $v = \pm 1$. Solitons are interacting, undergoing pairwise elastic scattering. The scattering is implemented as a Wigner time delay [40]. Precisely, when a left and a right moving soliton meet at the same site, they merge giving rise to the configuration $\dots 010 \dots$. The solitons remain “bound” together for a unit of time, before re-emerging as distinct left and right movers (several scattering processes are shown in Fig. 1). Again, this behavior is reminiscent of generic integrable models, which exhibit factorized two-body elastic scattering. The major difference is that in generic integrable models the quasiparticles possess a nontrivial dispersion, implying that their energies and velocities depend on a real parameter λ , which labels the different quasiparticles. It is important to stress that there is a mapping between the soliton basis and the standard bit basis. The mapping can be represented as an *MPO*. By applying the *MPO* on a generic string of bits, one obtains the corresponding configuration of left and right movers. Crucially, the mapping is local, because to determine whether at a generic site x there is a left or right moving soliton, only the bit configuration of the

neighboring sites is needed. This implies that the mapping can be represented as an *MPO* with finite bond dimension χ (see Ref. [14] and [15] for the explicit mapping). The bond dimension of the *MPO* that encodes the mapping does not depend on time, and cannot affect the leading behavior of the operator entanglement in the large time limit.

Let us now discuss operator spreading in the rule 54 chain. First, let us observe that the identity operator is

$$\mathbb{1} = \prod_x (|0\rangle\langle 0| + |1\rangle\langle 1|)_x, \quad (6)$$

where the subscript x means that the operator lives in the Hilbert space at site x . Upon expanding the product in (6), one obtains the equal-weight superposition of all the terms with an arbitrary number of projectors $|0\rangle\langle 0|$ and $|1\rangle\langle 1|$. The identity commutes with the evolution operator, meaning that the equal-weight superposition is mapped onto itself under the dynamics. The *MPO* representing the identity has bond dimension $\chi = 1$. This is evident from the fact that in the bit basis, irrespective of the local projector present at site x , the neighboring sites at $x + 1$ and $x - 1$ can have both $|0\rangle\langle 0|$ or $|1\rangle\langle 1|$. This implies that $S_n(\mathbb{1}) = 0$ for any n , and at any time.

The behavior changes dramatically if an operator \mathcal{O} is inserted at the center of the system, because the bond dimension of the *MPO* of the operator starts growing with time. Specifically, a double lightcone forms (see Fig. 1 (b)), as information propagates away from the operator insertion at finite velocity. The *MPO* of the operator has bond dimension $\chi = 1$ outside of the lightcone, where the operator remains the identity, whereas inside the lightcone its bond dimension grows. The reason is that the operator insertion puts nonlocal constraints on the motion of the left and right movers. To illustrate that, we now focus on the spreading of diagonal operators, for which the double-lightcone is symmetric, i.e., its upper part coincides with its lower one. Specifically we consider the local projector operator P_z acting at the center of the system, and $S_{L/2}^z$, defined as

$$P_z := \frac{1}{2} \left(\mathbb{1} + \sigma_{L/2}^z \right) = |1\rangle\langle 1|, \quad S_{L/2}^z := \sigma_{L/2}^z, \quad (7)$$

with σ_x^z the Pauli matrix acting at site $L/2$. Notice that while S^z is a traceless operator, P_z has a nonzero trace. Operator spreading is better understood in the soliton basis [14]. To represent P_z in the basis of left and right movers, it is convenient to expand $\mathbb{1}_{L/2-1} P_z \mathbb{1}_{L/2+1}$ as

$$\mathbb{1}_{L/2-1} P_z \mathbb{1}_{L/2+1} = |010\rangle\langle 010| + |011\rangle\langle 011| + |110\rangle\langle 110| + |111\rangle\langle 111|. \quad (8)$$

The first term in (8) creates a pair of scattering solitons (as depicted in Fig. 1 (b)), whereas the second and third one creates a left and a right moving soliton at the center, respectively. Upon applying the evolution operator (4) the solitons created by the insertion of the operator propagate, scattering with the background solitons away from

the center. This means that at a generic time t any allowed soliton configuration in the light cone has to contain the solitons that were created by the operator insertion at $t = 0$, although their positions are shifted by the scatterings with the background solitons (see Fig. 1 (b)). All the *allowed* soliton configurations at time t have the same amplitude. One can show that the bond dimension of the evolved *MPO* is determined by the number of steps to decide whether a generic soliton configuration in the lighthouse is allowed or not [24, 14]. Equivalently, this is the number of steps needed to identify the positions at time t of the solitons that emerged from the center of the chain, and it grows as t^2 . Importantly, the fact that $\chi = \mathcal{O}(t^2)$ provides only a bound on the growth of the *OSE* entropies. Indeed, by assuming that all the χ Schmidt values in (2) are the same, one obtains $S_1 \propto 2\ln(t)$. On the other hand, Ref. [14] provided numerical evidence that $S_1 \propto \ln(t)$ for the operator S^z and $S_1 \propto 1/2\ln(t)$ for P_z [15]. This means that the exact *MPOs* describing the dynamics of local operators contain too much information and can be further compressed. The reason why this is possible has not been clarified yet.

However, it has been argued in Ref. [15] that the growth of the *OSE* entropy reflects the diffusive quasiparticle spreading. Indeed, as a consequence of the interactions, the trajectory of the solitons (both the ones produced at the center and the background ones) exhibits diffusion. If one imagine of coarse graining the dynamics, one has that the effect of interactions, at long times and large distances, is a renormalization of the soliton velocities [17]. In the coarse-grained picture, the solitons move with their renormalized velocities as free particles, i.e., without scattering. Now, the dynamics resembles that of the identity operator, implying that the operator entanglement does not grow. This suggests that the growth of the *OSE* could be attributed to the diffusive fluctuations of the solitons trajectories.

2.2. Spin-1/2 *XXZ* chain and its nonintegrable deformation

In this work we also consider a nonintegrable deformation of the spin-1/2 Heisenberg *XXZ* chain defined by the Hamiltonian

$$H = \sum_{x=1}^{L-1} \frac{1}{2} (S_x^+ S_{x+1}^- + S_x^- S_{x+1}^+) + \Delta \sum_{x=1}^{L-1} S_x^z S_{x+1}^z + \Delta' \sum_{x=1}^{L-2} S_x^z S_{x+2}^z. \quad (9)$$

Here S_x^\pm are standard raising/lowering spin-1/2 operators acting at site x , and Δ, Δ' are real parameters. For $\Delta = \Delta' = 0$ the model (9) can be mapped to a system of noninteracting fermions. For $\Delta' = 0$, Eq. (9) becomes the *XXZ* chain, which is a prototypical Bethe ansatz solvable model [41]. For nonzero Δ' the model is nonintegrable, as one can show by studying the statistics of the gaps in the energy spectrum [15]. Notice that Eq. (9) commutes with the total magnetization $M = \sum_x S_x^z$, also for nonzero Δ' . As for the rule 54 chain, we focus on the spreading of the diagonal operators S^z and P_z , defined in (7). The *XXZ* chain possesses well-defined quasiparticles, which are at the heart of the quasiparticle picture [5, 42] for entanglement spreading and of Generalized Hydrodynamics [43, 44]. In contrast with the rule 54 chain,

for which one can construct explicitly the *MPO* describing a generic time-dependent operator, it is much more challenging to obtain exact results for operator spreading in the *XXZ* chain (9), even in the integrable case for $\Delta' = 0$. However, it has been numerically shown in Ref. [14] that for $\Delta' = 0$ the *OSE* entropy grows logarithmically with time for generic Δ . In particular, Ref. [15] showed that for $\Delta' = 0$, $S_1(P_z)$ grows as $1/2 \ln(t)$, for any Δ , which is the same behavior observed in the rule 54 chain. The dynamics of $S_1(S^z)$ is compatible with a logarithmic growth as $S_1(S^z) \approx \ln(t)$. Finally, for $\Delta' \neq 0$, numerical results for the growth of the *OSE* are inconclusive due to strong finite-time effects [15].

3. Analytical bounds on the growth of the *OSE* entropies

Let us now discuss some analytical results that are available for the *OSE* entropies in generic systems. In Section 3.1 we review the result of Ref. [38], showing that the *OSE* entropies of a given operator \mathcal{O} can be bound by its Infinite Temperature Auto Correlator (*ITAC*). In Section 3.2, following Ref. [26] we argue that the *OSE* of an operator is determined by its traceless part. Finally, in Section 3.3 we review the results of Ref. [15] trying to establish a relationship between the growth of *OSE* and diffusion.

3.1. Operator entanglement and *ITAC*: The bound of Ref. [38]

Ref. [38] showed that for $n > 1$ the Rényi *OSE* entropies $S_n(\hat{\mathcal{O}})$ of a generic local operator $\hat{\mathcal{O}}$ is bound by its *ITAC* as

$$S_n(\hat{\mathcal{O}}) \leq \frac{2n}{1-n} \ln |\langle \hat{\mathcal{O}}^\dagger(t) \hat{\mathcal{O}}(0) \rangle_{T=\infty}| = \frac{2n}{1-n} \ln |\text{Tr}(\hat{\mathcal{O}}^\dagger(t) \hat{\mathcal{O}}(0))|, \quad n > 1, \quad (10)$$

where we used that $\langle \hat{\mathcal{O}}_1 \hat{\mathcal{O}}_2 \rangle_{T=\infty} = \text{Tr}(\hat{\mathcal{O}}_1 \hat{\mathcal{O}}_2)$. The derivation of (10) is straightforward, and we report it for completeness. One starts from the decomposition

$$\frac{\hat{\mathcal{O}}(t)}{\sqrt{\text{Tr}(\hat{\mathcal{O}}^\dagger \hat{\mathcal{O}})}} = \sum_{rs} \Lambda_{rs}(t) \hat{\mathcal{O}}_{r,A} \otimes \hat{\mathcal{O}}_{s,B}, \quad (11)$$

where Λ_{rs} is a time-dependent matrix, and $\hat{\mathcal{O}}_{r,A}$ and $\hat{\mathcal{O}}_{s,B}$ form two time-independent orthonormal bases for the operators with support in A and B , i.e., satisfying $\text{Tr}(\hat{\mathcal{O}}_{r,A(B)}^\dagger \hat{\mathcal{O}}_{r',A(B)}) = \delta_{rr'}$. One can perform a Singular Value Decomposition of Λ_{rs} to obtain

$$\frac{\hat{\mathcal{O}}(t)}{\sqrt{\text{Tr}(\hat{\mathcal{O}}^\dagger \hat{\mathcal{O}})}} = \sum_r \sqrt{\lambda_r(t)} \hat{\tilde{\mathcal{O}}}_{r,A}(t) \otimes \hat{\tilde{\mathcal{O}}}_{r,B}(t), \quad (12)$$

where $\sqrt{\lambda_r}$ are the Schmidt values, and the operators appearing in the right-hand side of (12) depend on time and are orthonormal. Notice that the singular values (Schmidt values) are in one-to-one correspondence with the eigenvalues of the reduced density

matrix of one of the subsystems, and hence they are independent on the basis used to define Λ_{rs} . We now obtain the chain of inequalities as [38]

$$\begin{aligned} |\langle \hat{\mathcal{O}}^\dagger(t) \hat{\mathcal{O}}(0) \rangle_{T=\infty}| &= |\text{Tr}(\Lambda^\dagger(t) \Lambda(0))| \leq \left| \sum_k \sqrt{\lambda_k(t) \lambda_k(0)} \right| \\ &\leq \kappa_0 \left(\sum_k \frac{\sqrt{\lambda_k(0)}}{\kappa_0} \lambda_k^{n/2} \right)^{1/n} \leq \kappa_0^{1-1/n} \left(\sum_k \lambda_k^n \right)^{1/(2n)}, \quad \kappa_0 := \sum_k \sqrt{\lambda_k(0)}. \end{aligned} \quad (13)$$

In the first row in (13) we used the von Neuman trace inequality [45] $|\text{Tr}(XY)| \leq \sum_j \alpha_j \beta_j$, with α_j, β_j the singular values obtained from the Schmidt decomposition of X and Y , respectively. In the second row of (13) we employed the Jensen inequality

$$\varphi \left(\frac{\sum_k a_k x_k}{\sum_k a_k} \right) \geq \frac{\sum_k a_k \varphi(x_k)}{\sum_k a_k}, \quad \forall \varphi(x) \text{ concave}, \quad (14)$$

where we used $\varphi(x) = x^{1/n}$, $x_k = \lambda_k^{n/2}$, and $a_k = \sqrt{\lambda_k(0)}$. We also used that $x^{1/n}$ is concave for $n > 1$. In the last step we used the Cauchy-Schwartz inequality

$$\sqrt{\sum_k u_k v_k} \leq \sqrt{\sum_k u_k^2} \sqrt{\sum_k v_k^2}, \quad (15)$$

with $u_k = \sqrt{\lambda_k(0)}/\kappa_0$, and $v_k = \lambda_k^{n/2}$. In deriving (13) we also used $\sum_k \lambda_k(0) = 1$. For local product operators the Schmidt decomposition at $t = 0$ is trivial with only one Schmidt value $\lambda = 1$, implying $\kappa_0 = 1$. By taking the logarithm of both members of (13) and multiplying them by $2n/(1-n)$, one obtains (10).

Let us now focus on the *ITAC* on the left-hand side of (10). One should expect a vanishing behavior in the limit $t \rightarrow \infty$, although several scenarios are possible. Ballistic spreading of operators, as in integrable systems, suggests power-law [46] decay as $1/t$ in the limit $t \rightarrow \infty$, whereas diffusive spreading corresponds to the slower decay as $1/\sqrt{t}$. From (10), power-law decay of the *ITAC* implies a logarithmic growth of the *OSE*. On the other hand, for some operators the *ITAC* in (10) decays exponentially with time. For instance, this happens for the correlator $\langle S^+(t) S^- \rangle_{T=\infty}$ in the *XX* spin chain [47]. In these situations, Eq. (10) gives a linear bound for the *OSE* entropies. However, the bound (10) is generically not saturated. For instance, it is well-known that in the *XX* chain the *OSE* entropy of S^+ grows logarithmically with time [12, 11, 13]. Similarly, by assuming that Eq. (10) is saturated for S^z , one has a logarithmic growth of the *OSE*, as $S_n(S^z) \sim 2n/(n-1) \ln(t)$ since $\langle S^z(t) S^z(0) \rangle \sim 1/t$ at long times [47]. On the other hand, it is well-known that $S_n(S^z)$ saturates to a constant at long times [12, 13]. We conclude that Eq. (10) is in general a loose bound on the *OSE* growth.

3.2. Traceless versus traceful operators (Ref. [26])

Following Ref. [26], one can argue that the dynamics of $S_n(\hat{\mathcal{O}})$ can be obtained from $S_n(\hat{\mathcal{O}}')$, where $\hat{\mathcal{O}}'$ is the traceless part of $\hat{\mathcal{O}}$. Let us decompose the generic normalized operator $\hat{\mathcal{O}}$ as

$$\hat{\mathcal{O}} := \sqrt{p} \mathbb{1} + \sqrt{1-p} \hat{\mathcal{O}}' \quad \sqrt{p} := \text{Tr}(\hat{\mathcal{O}}), \quad (16)$$

where $\hat{\mathcal{O}}'$ is traceless and both $\hat{\mathcal{O}}'$ and $\mathbb{1}$ are normalized. The time-evolved operator $\hat{\mathcal{O}}(t)$ can be decomposed as

$$\hat{\mathcal{O}}(t) := \sqrt{p}\mathbb{1} + \sqrt{1-p}\hat{\mathcal{O}}'(t), \quad (17)$$

and $\hat{\mathcal{O}}'(t)$ is traceless, since the dynamics preserves the trace. After performing a Schmidt decomposition of $\hat{\mathcal{O}}'$, we obtain

$$\hat{\mathcal{O}}(t) = \sqrt{p}\mathbb{1}_A \otimes \mathbb{1}_B + \sum_i \sqrt{(1-p)\lambda'_i(t)} \hat{\mathcal{O}}'_{A,i}(t) \otimes \hat{\mathcal{O}}'_{B,i}(t), \quad (18)$$

where $\lambda'_i(t) \geq 0$ are the Schmidt values. As discussed in Ref. [26] while at $t = 0$ the Schmidt decomposition in (16) is exact, the decomposition for $\hat{\mathcal{O}}(t)$ is only approximate. The reason is that the time-evolved operators $\hat{\mathcal{O}}'_{i,A}(t)$ are not traceless.

In general one should expect that at least some of the operators $\hat{\mathcal{O}}'_{A,i}$ appearing in the second term in (18), and which are initially traceless, will develop a nonzero trace with time. This implies that they will not be orthogonal to the identity $\mathbb{1}_A$, which makes it apparent that Eq. (18) is not a Schmidt decomposition for $\hat{\mathcal{O}}(t)$. If we assume that all the $\hat{\mathcal{O}}'_{A,i}$ are traceless, then Eq. (18) is a Schmidt decomposition for $\hat{\mathcal{O}}(t)$. Although this is an approximation, it is natural to expect (see section 5.1) that the probability that the dynamics generates the identity operator in all the sites of A rapidly decays with the size of A , meaning that the decomposition (18) will become asymptotically exact in the limit $t \rightarrow \infty$ if A is the semi-infinite system.

This implies that the operator entanglement spectrum $\{\lambda_i\}$ of $\hat{\mathcal{O}}(t)$ can be decomposed as

$$\{\lambda_j\} = \{p\} \cup \{(1-p)\lambda'_i\}, \quad (19)$$

where λ_i are the same as in (18). Eq. (20) implies that the OSE of a given operator $\hat{\mathcal{O}}$ can be determined by that of its traceless part $\hat{\mathcal{O}}'$. Specifically, for the von Neumann entropy one has

$$S(\hat{\mathcal{O}}) = p \ln(p) + (1-p) \sum_i \lambda'_i \ln(1-p) + (1-p) S(\hat{\mathcal{O}}') = p \ln(p) + (1-p) \ln(1-p) + (1-p) S(\hat{\mathcal{O}}'), \quad (20)$$

where in the last step we used that $\sum_i \lambda'_i = 1$.

Similarly, the Rényi entropy satisfy

$$S_n(\hat{\mathcal{O}}) = \frac{1}{1-n} \ln \left[p^n + (1-p) \sum_i \lambda_i^n \right] \approx \frac{n}{1-n} \ln(p), \quad (21)$$

where we used that at long times $\sum_i \lambda_i^n \rightarrow 0$ because the operator support increases, while $\sum_i \lambda_i = 1$ because the operators are normalized. As we will discuss in Section 4 and Section 5, the decomposition (19) captures correctly the dynamics of the OSE, at least at long times and for large subsystems A .

3.3. Operator space entanglement and diffusion (Ref. [15])

Inspired by the results for the rule 54 chain, a plausible scenario is that the dynamics of the operator entanglement reflects the diffusive dynamics of the underlying solitons [15], as discussed already in Section 2.1. Again, at a ballistic level, or at a coarse-grained level, the left and right movers behave as noninteracting particles, moving with effective velocities, which are determined by the scatterings. This also applies to the solitons produced at the center of the chain by the operator insertion. Since at a ballistic level the solitons behave as free particles, the operator entanglement does not grow [48]. Still, it is challenging to encapsulate this idea in a quantitative framework. As suggested in Ref. [15], a crude approximation for the Schmidt decomposition of an operator \hat{O} is

$$\hat{O}(t) = \sum_{k=0}^{t-|x|} \frac{\sqrt{\binom{t-|x|}{k} \binom{t+|x|}{t-k}}}{\sqrt{\binom{2t}{t}}} \hat{O}_{A,k} \otimes \hat{O}_{B,t-k}. \quad (22)$$

In (22), $\hat{O}_{A,k}$ and $\hat{O}_{B,t-k}$ are normalized operators in A and B constructed with k and $t-k$ solitons. In (22) we assume that $\hat{O}_{A,k}$ and $\hat{O}_{B,t-k}$ are some “flat” superpositions of all the configurations with k and $t-k$ solitons. Physically, this means that the scatterings maximally “scramble” the trajectories of the solitons within the lightcone. In (22), x is the position of the cut dividing subsystem A from B (see Fig. 1). The two binomials in (19) are the number of ways of arranging the solitons in A and B . In the limit $t \rightarrow \infty$ the coefficients in (22) are dominated by the term with $k = (t - |x|)/2$, with diffusive fluctuations as \sqrt{t} . Now, the decomposition in (22) is an approximation because interactions are local and the trajectories of the solitons cannot be scattered at arbitrary distances. The bond dimension of the decomposition in (19) is $t - |x| + 1$. Notice that $t - |x|$ is the largest number of solitons that can be accommodated within A . Notice also that Eq. (22) implies that there are only $\propto t$ nonzero Schmidt values, whereas the exact *MPO* describing the dynamics of generic operators has $\sim t^2$ nonzero Schmidt values [14]. By using (22), one obtains the analytical result for the von Neumann entropy as

$$S_n = \frac{1}{2} \ln(t), \quad \forall n. \quad (23)$$

Thus, Eq. (22) implies that the Rényi *OSE* entropies should not depend on n . The prefactor $1/2$ of the logarithmic growth clearly reflects the diffusive spreading of the solitons trajectories. As it will be clear in the following, S_n depend on n , signaling that Eq. (22) does not capture correctly the detailed structure of the operator entanglement spectrum. On the other hand, Eq. (23) is in agreement with the growth of the von Neumann entropy of the projector operator P_z (see Ref. [15]).

4. Rényi entanglement of operators in the rule 54 chain: A *tDMRG* analysis

Here we discuss *tDMRG* results for S_n of diagonal operators in the rule 54 chain. In particular, in Section 4.1 we show that given an operator \hat{O} with nonzero trace, $S_1(\hat{O})$

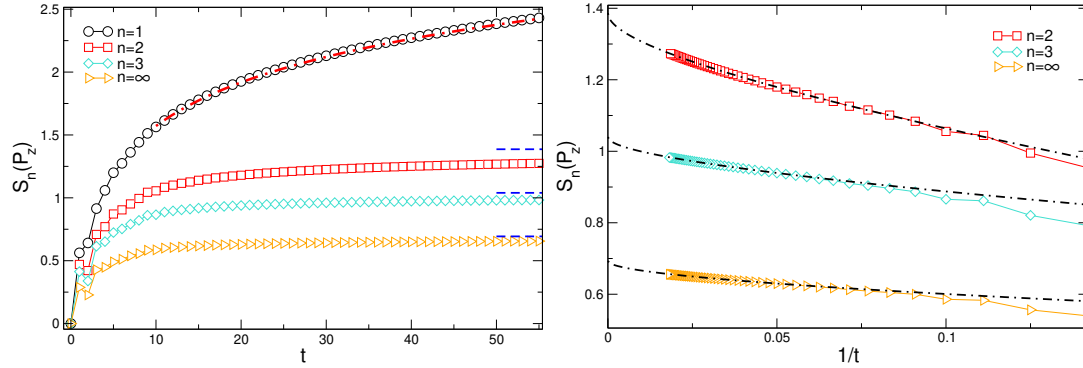


Figure 2. Dynamics of the Rényi operator entanglement entropies S_n for the projector operator P_z in the rule 54 chain. Left panel: $tDMRG$ data for S_n plotted versus time t for several values of n . The dashed-dotted line is the behavior $S_1 = a \ln(t) + b$, with a, b a fitting parameter. The fit gives $a = 0.50(1)$. The horizontal lines are $S_n = n/(n-1) \ln(p)$ (cf. Eq. (21)) with $p = 1/2$. Right panel: Same data as in the left panel plotting $S_n - n/(n-1) \ln(2)$ versus $1/t$ for $n > 1$. The dashed-dotted lines are fits to $S_n = n/(n-1) \ln(2) + a_1/t^{1/2} + a_2/t$, with a_1, a_2 fitting parameters.

can be obtained from $S_1(\hat{\mathcal{O}}')$, with $\hat{\mathcal{O}}'$ the traceless part of the operator. Moreover, we show that S_n saturate to a constant value in the limit $t \rightarrow \infty$, in agreement with the results of Section 3.2. In Section 4.2 we focus on traceless operators. We numerically show that S_n is compatible with a logarithmic growth for any n , although the prefactor of the logarithmic growth depends on n in a nontrivial manner. Finally, in Section 4.3 we discuss how this is reflected in the distribution of the levels of the operator entanglement spectrum.

4.1. Dynamics of the Rényi entropies for P_z : Effect of a nonzero trace

In Fig. 2 we show $tDMRG$ data for S_n of the spin projector operator P_z (cf. (7)). Our $tDMRG$ simulations are performed at fixed bond dimension $\chi = 1600$, which allows us to reach times $t \approx 60$. As it is clear from Fig. 2 (left panel), $S_n(P_z)$ increase with time, although the dynamics is much slower for $n > 1$, as compared with $n = 1$. The growth of $S_1(P_z)$ was investigated in Ref. [14] and Ref. [15], and it is compatible with the behavior $S_1(P_z) \sim 1/2 \ln(t)$, i.e., Eq. (23). The dashed-dotted line in the left panel of Fig. 2 is

$$S_n = a \ln(t) + b, \quad (24)$$

with a, b fitting parameters. To obtain a, b we fitted the data in the range $t_{min} \leq t \leq 50$ to (24), i.e., discarding the short times with $t \leq t_{min}$ because Eq. (24) is valid only at asymptotically long times. We estimated the error on a by monitoring its variation when increasing t_{min} . We should observe that by fitting the data for $n > 1$ to (24) we obtain quite “small” values for a as $a \approx 0.08, 0.04, 0.02$ for $n, 2, 3, \infty$. However, as we now discuss, this signals that Eq. (24) does not apply for $n > 1$, and S_n saturates for $t \rightarrow \infty$, as discussed in section 3.2. The saturation values predicted by (21) are reported as horizontal dashed lines in Fig. 2. The deviations from (21) have to be interpreted

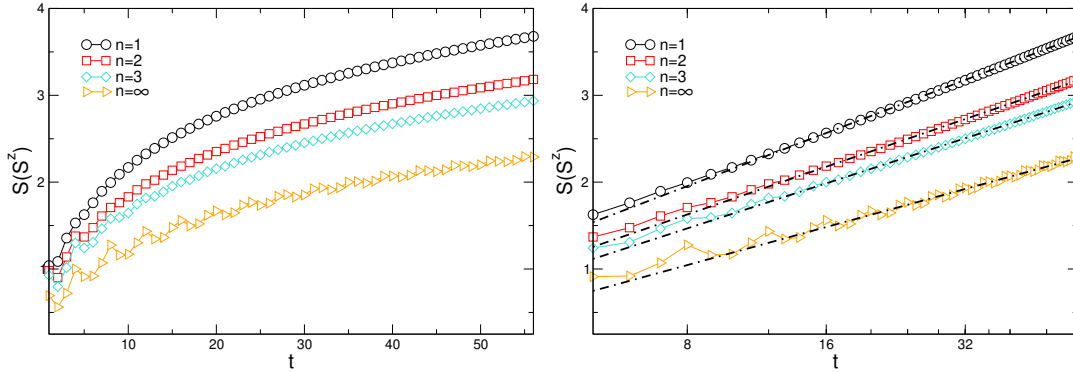


Figure 3. Dynamics of the Rényi operator entanglement entropies S_n for S^z in the rule 54 chain. Left panel: $tDMRG$ data for S_n plotted versus time t and $n = 1, 2, 3, \infty$. Right panel: Same as in the left panel using the logarithmic scale on the x -axis. The dash-dotted lines are fits to $S_n = a \ln(t) + b$, with a, b fitting parameters.

as finite-time corrections. Corrections are more precisely investigated in the right panel of Fig. 2 plotting $S_n - n/(n-1) \ln(2)$ versus $1/t$. A fit of the data at long times to the behavior $\sim t^{-\alpha}$ gives $\alpha \approx 1/2$. This motivates the ansatz for S_n as

$$S_n = \frac{n}{n-1} \ln(2) + \frac{a_1}{t^{1/2}} + \frac{a_2}{t}, \quad (25)$$

with a_1, a_2 fitting parameters. As it is clear from Fig. 2, the fits are in satisfactory agreement with the numerical data, confirming that S_n saturate to a constant in the limit $t \rightarrow \infty$. We anticipate that the saturating behavior of S_n for $n > 1$ is also confirmed by the behavior of the operator entanglement spectrum (see Section 4.3).

4.2. Non CFT scaling of the OSE of traceless operators?

Having discussed the Rényi entropies of P_z , we now focus on its traceless part S^z . In Fig. 3 we show $tDMRG$ data for the rule 54 chain. Our data are obtained by employing bond dimension $\chi = 1600$. In contrast with the projector operator P_z (see Fig. 2), now S_n grow logarithmically also for $n > 1$. This is confirmed in the right panel of Fig. 3 plotting S_n versus time by using a logarithmic scale on the x -axis. The dashed-dotted lines in Fig. 3 are fits to the behavior (24). We now obtain $a = 0.92(2), 0.80(5), 0.76(5), 0.64(5)$ for $n = 1, 2, 3, \infty$. Notice that for $n = 1$ the fit gives $a = 0.92(2)$, which appears to be different from $a = 1$. This is also in contrast with what one should expect from (20), which would give $a \approx 1$ since for P_z one has $a \approx 0.5$. Still, the discrepancy could be attributed to the systematic error due to finite-time corrections.

Let us consider the scaling of the moments M_n of the λ_i (cf. (2)), which form the operator entanglement spectrum. M_n are defined as

$$M_n := \sum_i \lambda_i^n. \quad (26)$$

Clearly, M_n contain the same information about the distribution of the ES levels as the Rényi entropies. The moments M_n for the operator S_z are plotted in Fig. 4. In

the Figure we show M_n versus time for several values of n , employing a logarithmic scale on both axis. First, the data exhibit a clear power-law behavior with increasing t . Moreover, for $n < 1$, M_n increases with time, whereas for $n > 1$, M_n vanishes in the limit $t \rightarrow \infty$. The exponent of the power-law depends on n , reflecting that the prefactor of the logarithmic growth of S_n depends on n (see Fig. 4). For $n = 1$, one has the normalization $M_1 = 1$ (not shown in the Figure). In the limit $n \rightarrow \infty$ a fit to the power-law behavior suggests the decay as $t^{-2/3n}$. The large n limit is confirmed in the inset of Fig. 4, where we plot λ_1 versus t . The dotted and the dashed-dotted lines are the behaviors as $t^{-1/2}$ and $t^{-2/3}$, respectively.

Let us assume that M_n for large t have the power-law behavior as

$$M_n \sim t^{-f_n}. \quad (27)$$

It is natural to conjecture that f_n is of the form

$$f_n = na_0 + \frac{a_1}{n} + \frac{a_2}{n^2} + \dots, \quad (28)$$

where the dots are for higher powers of $1/n$. Eq. (28) is reminiscent of the *CFT* scaling of the moments of the ground-state ES spectrum [39]. Precisely, in *CFT*s one has that only a_0 and a_1 are nonzero, and $a_1 = -a_0$, with a_0 related to the central charge of the *CFT*. Let us now consider the limit $n \rightarrow 1$ to recover the von Neumann *OSE*. If we assume that only a_0, a_1 are nonzero in (28), one has $S_1 \sim 2a_0 \ln(t)$. Fig. 3 suggests the behavior $S_1 \sim \ln(t)$, whereas from Fig. 4 we have $\lambda_1 \sim t^{-2/3}$, implying $a_0 > 1/2$. This discrepancy could signal that the terms a_j with $j > 1$ in the expansion (28) are nonzero. Finally, we should stress that *CFT*-like scaling was demonstrated for the growth of Rényi entropies of string operators in the *XX* chain [13].

4.3. Operator entanglement spectrum (ES)

Let us now consider the operator entanglement spectrum (*ES*). The levels ξ_i of the *ES* are defined as

$$\xi_i = -\ln(\lambda_i), \quad (29)$$

with λ_i the squared singular values in (2). In Fig. 5 we focus on the dynamics of the entanglement spectrum of P_z and of S^z (left and right panels, respectively). Notice that P_z and S^z differ by $1/2\mathbb{1}$, and the results of Section 3.2 should hold. The *ES* levels exhibit a nontrivial dynamics. Upon increasing time, there are more and more levels that contribute to the *ES*. Let us focus on the operator entanglement spectrum of P_z (left panel in Fig. 5). The smallest *ES* level is $-\ln(\lambda_1) \approx \ln(2)$, reflecting the behavior $S_\infty \rightarrow \ln(2)$ for $t \rightarrow \infty$, which we observed in Fig. 3 (right panel). The *ES* levels above the lowest one are strongly suppressed. For instance, for $t = 40$ they are $-\ln(\lambda_2) \approx 2.7$. This is in agreement with the decomposition (19).

Moreover, according to (19) one can obtain the operator *ES* of P_z from that of S^z . Indeed, one should expect that (cf. (19))

$$\lambda_i = \left\{ \frac{1}{2}, \frac{1}{2} \lambda'_i \right\}, \quad (30)$$

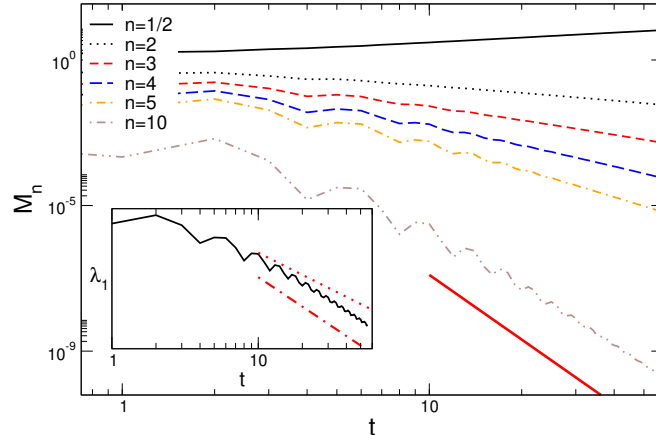


Figure 4. Moments M_n of the squared singular values λ_i (cf. (2)) for the dynamics of the operator S^z in the rule 54 chain. We plot M_n as functions of time t and for several values of n . Notice the logarithmic scale on both axes. The thick red line is the behavior $t^{-2/3n}$ for $n = 10$. The inset shows the largest Schmidt value λ_1 as a function of t . The dotted line and the dashed-dotted lines are the behaviors $t^{-1/2}$ and $t^{-2/3}$, respectively.

with $-\ln(\lambda_i)$ forming the *ES* of S^z and $-\ln(\lambda_i)$ that of P_z . The operator *ES* of S^z is reported in the right panel in Fig. 5. Now the *ES* level $\lambda_1 = \ln(2)$ is not present, in contrast with the *ES* of P_z (left panel in the Figure). In the inset we show the *ES* levels for S^z for $t = 20, 40$ (empty symbols). These are the same data reported in the main Figure. We also show the shifted levels $-\ln(\lambda_i) - \ln(2)$ with λ_j forming the *ES* of P_z . Interestingly, they match the *ES* of S^z quite accurately, and the agreement improves at longer times. As anticipated, the results of Fig. 5 confirm that although the decomposition in (19) is an approximation because $\hat{\mathcal{O}}'_{i,A}(t)$ (cf. (18)) have nonzero trace at $t > 0$, it becomes exact in the limit $t \rightarrow \infty$. This is due to the fact that it is “unlikely” that the dynamics gives rise to a string of identity operators in the full subsystem A .

Finally, it is interesting to discuss the distribution of *ES* levels. Since the *ES* of operators with nonzero trace can be derived from that of their traceless part, we focus on S^z . We consider the number of *ES* levels $n(\lambda)$, which are larger than λ . In critical ground states described by *CFT*s, it has been shown that [39]

$$n(\lambda) = I_0(2\xi), \quad \xi := \sqrt{b \ln(\lambda_M/\lambda)}, \quad (31)$$

where λ_M is the largest eigenvalue of the *ES*, $b = -\ln(\lambda_M)$, and I_0 is the modified Bessel function of the first kind. Eq. (31) implies that $n(\lambda)$ is “superuniversal”, because it depends only on the central charge of the *CFT*, which is encoded in the scaling of λ_M .

In Fig. 6 we plot $n(\lambda)$ as a function of ξ . The different symbols correspond to different times. At long times the data exhibit scaling collapse. This could suggest that although the moments M_n do not scale as in *CFT* (see Fig. 6), $n(\lambda)$ is a function of ξ , at least in the limit $t \rightarrow \infty$. The dashed line in Fig. 6 is the prediction in *CFT* systems

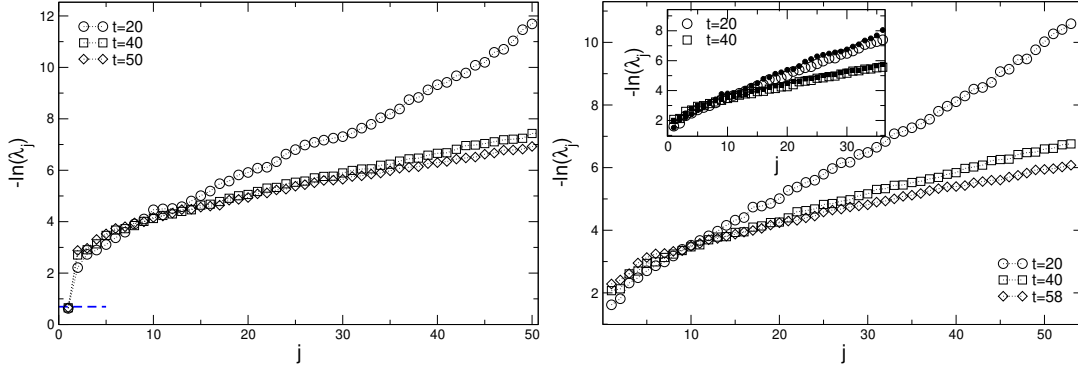


Figure 5. Dynamics of the operator entanglement spectrum in the rule 54 chain. Both panels show $tDMRG$ results with bond dimension $\chi = 1600$. Left panel: Operator entanglement spectrum for the projector operator P_z . The y -axis shows $-\ln(\lambda_j)$, with λ_j the squared Schmidt values. On the x -axis j is a label for the entanglement spectrum levels. The different symbols are for different times. Right panel: Same as in the left panel for the operator S^z . Inset: Comparison between the ES levels $-\ln(\lambda'_j)$ of S^z (empty symbols) and the shifted ES levels $-\ln(\lambda_j) - \ln(2)$ of P_z .

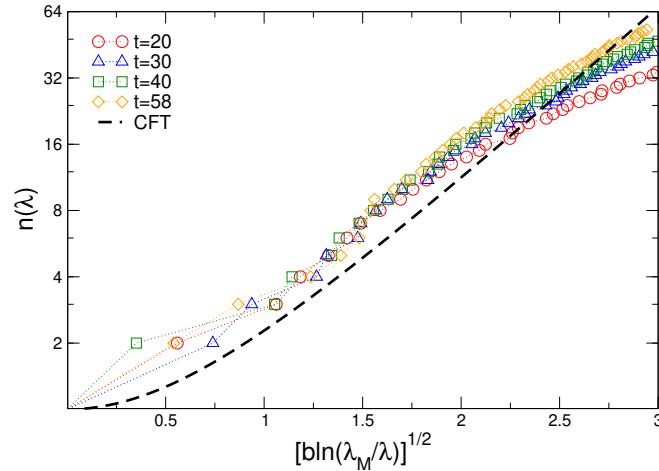


Figure 6. Dynamics of the operator entanglement spectrum levels in the rule 54 chain. We show $tDMRG$ data at fixed bond dimension $\chi = 1600$ for the operator S^z . We plot $n(\lambda)$, i.e., the number of ES levels smaller than λ , as a function of the scaling variable $\xi = \sqrt{b \ln(\lambda_M/\lambda)}$, with $b := -\ln(\lambda_M)$, and $-\ln(\lambda_M)$ the lowest ES level. Different symbols correspond to different times. The dashed line is (31), i.e., the CFT-like scaling.

$n(\lambda) = I_0(2\xi)$ (cf. (31)). Fig. 6 shows strong deviations from (31). This reflects that the moments M_n (cf. (27)) do not obey CFT scaling, which is given by Eq. (28) with $a_j = 0$ for $j > 1$ and $a_1 = -a_0$.

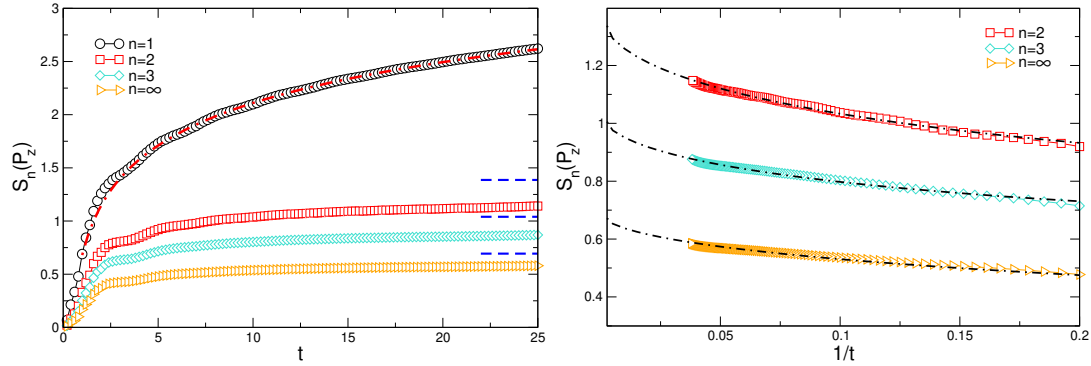


Figure 7. Dynamics of the Rényi operator entanglement entropies S_n for the projector operator P_z in the XXZ spin chain with $\Delta = 10$. Left panel: $tDMRG$ data for S_n plotted versus time t . The dashed-dotted line is a fit to $S_1 = a \ln(t) + b$, with a, b fitting parameters. For $n = 1$ the fit gives $a \approx 1/2$. The dashed lines are (21). Right panel: Same as in the left panel using the logarithmic scale on the x -axis. The dashed-dotted lines are fits to $S_n = n/(n-1) \ln(2) + a_1/t^{1/2} + a_2/t$, with a_1, a_2 fitting parameters.

5. Rényi OSE entropies in the deformed XXZ chain: $tDMRG$ results

We now focus on the operator spreading in the deformed XXZ chain (cf. (9)). We first consider the integrable case with $\Delta' = 0$, i.e., the XXZ chain. In section 5.1 we show that the decomposition (19) holds true also for the XXZ chain, similar to the rule 54 chain (see section 4.1). In section 5.2 we investigate the effect of Δ' , which breaks the integrability. Finally, in section 5.3 we investigate revivals in the OSE entropies in finite-size systems, showing that they can distinguish integrable from non-integrable dynamics.

5.1. Traceless versus operators with nonzero trace

Let us consider the Rényi entropies S_n of the projector operator P_z in the XXZ chain. We report $tDMRG$ data in Fig. 7 plotting $S_n(P_z)$ versus time for $n = 1, 2, 3, \infty$. The data are for the XXZ chain with $\Delta = 10$. Clearly, $S_1(P_z)$ increases logarithmically with time (see left panel in Fig. 7). The dashed-dotted line in the figure is a fit to the behavior $S_1 = a \ln(t) + b$, with a, b fitting parameters. The fit gives $a \approx 1/2$ in agreement with the results of Ref. [15]. For $n > 1$, the dynamics of S_n is compatible with a saturation at $t \rightarrow \infty$, similar to the rule 54 chain (see Section 4). In the right panel of Fig. 7 we plot $S_n - n/(n-1) \ln(2)$ versus $1/t$ for $n = 2, 3, \infty$. The dashed dotted lines are fits to

$$S_n = \frac{n}{n-1} \ln(2) + \frac{a_1}{t^{1/2}} + \frac{a_2}{t}, \quad (32)$$

with a_1, a_2 fitting parameters. The behavior of the corrections as $1/t^{1/2}$ is motivated by the results for the rule 54 chain (see Fig. 2). The dashed-dotted lines are obtained by fitting the data in the interval $1/t \in (0, .1]$. The agreement with (32) is satisfactory, confirming that the data are compatible with $S_n(t) \rightarrow n(n-1) \ln(2)$ for $t \rightarrow \infty$.

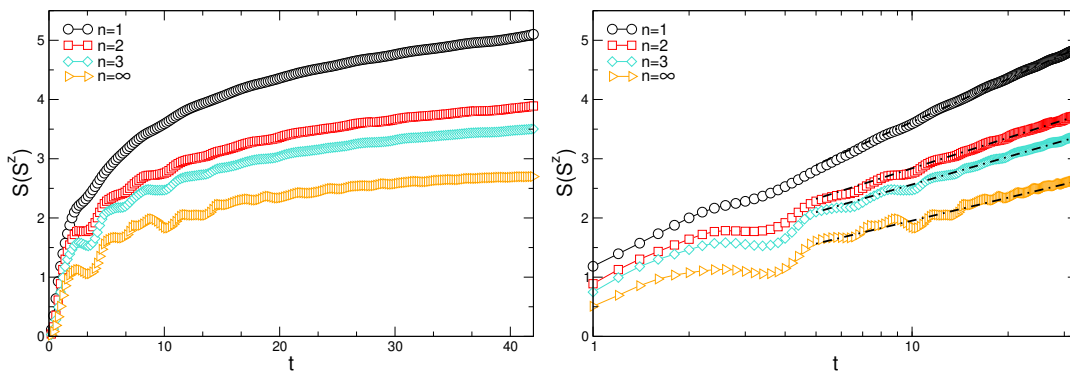


Figure 8. Dynamics of the Rényi operator entanglement entropies S_n for the operator S_z in the XXZ spin chain with $\Delta = 10$. Left panel: $tDMRG$ data for S_n plotted versus time t . Right panel: Same as in the left panel using the logarithmic scale on the x -axis. The dash-dotted lines are fits to (33).

Let us now consider the operator S^z . In Fig. 8 we show $tDMRG$ data for S_n for the XXZ chain with $\Delta = 10$. In contrast with the case of P_z the left panel of Fig. 8 suggests that S_n grows with time for any n , as for the rule 54 chain. This is supported in the right panel of Fig. 8 plotting S_n versus t and using a logarithmic scale on the x axis. The dashed-dotted lines in Fig. 8 are fits to

$$S_n = a \ln(t) + b + \frac{c}{t^{1/2}}, \quad (33)$$

with a, b, c fitting parameters. By fitting the data with $t > 10$ we obtain $a = 1.05(5), 0.70(5), 0.66(5), 0.50(5)$ for $n = 1, 2, 3, \infty$. Interestingly, the fitted values of a are consistent with the results obtained for the rule 54 chain (see Section 4), although the time scales that are accessible are not enough to clarify whether they are the same.

It is interesting to discuss the validity of the bound in Eq. (10), and whether it is saturated. Given an operator \hat{O} with $ITAC$ as $\langle \hat{O}(t)\hat{O}(0) \rangle_{T=\infty} \sim t^{-\alpha}$, with $\alpha > 0$, if we assume that the bound (10) is saturated we obtain

$$S_n \sim \frac{2\alpha n}{n-1} \ln(t). \quad (34)$$

For $\alpha = 1$ and $\alpha = 1/2$, which correspond to ballistic and diffusive operator spreading, Eq. (34) gives $S_n \sim 2n/(n-1) \ln(t)$ and $S_n \sim n/(n-1) \ln(t)$, respectively. Now, for $n = 2$, Eq. (34) implies that $S_2 \sim 4 \ln(t)$ and $S_2 \sim 2 \ln(t)$ for $\alpha = 1$ and $\alpha = 1/2$, respectively. On the other hand, from Fig. 8 one obtains the milder increase as $S_2 \sim 0.8 \ln(t)$. This confirms that the bound (10) is not saturated, at least for integrable systems.

5.2. Breaking integrability

For generic nonintegrable systems, according to the membrane picture for entanglement spreading, S_1 grows linearly with time [26]. The key assumption of the membrane picture is that the entanglement profile $S_1(x, t)$, with x denoting the position of

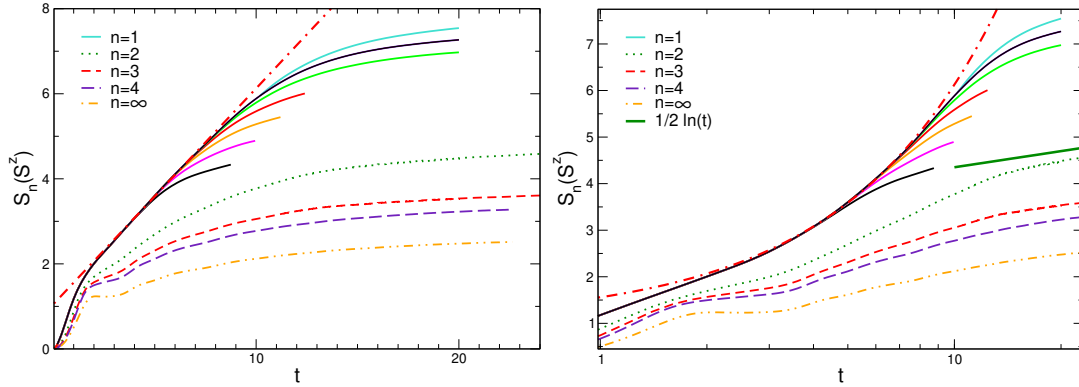


Figure 9. Dynamics of the Rényi operator entanglement entropies S_n for S^z in the nonintegrable XXZ chain with $\Delta = 3$ and $\Delta' = 0.25\Delta$ (cf. (9)). Left panel: t DMRG data for S_n as a function of time t . For $n = 1$ (continuous lines) the different curves correspond to different bond dimensions $\chi = 50, 100, 200, 400, 800, 1600, 2500$ (from bottom to top). The dash-dotted line is to highlight linear behavior at short times. The remaining curves are S_n with $n = 2, 3, 4, \infty$. For $n > 1$ we show data for $\chi = 1600$. Right panel: Same data as in the left panel using the logarithmic scale on the x -axis.

the cut dividing subsystem A and B (see Fig. 1), satisfies an equation of the form $\partial_t S_1(x, t) = s_{\text{eq}} \Gamma(\partial_x S_1(x, t))$, with Γ the entropy production rate, and s_{eq} the density of entanglement entropy at equilibrium [25]. Under quite general assumptions on Γ , the membrane picture predicts linear growth of the entropy. On the other hand, as it was stressed in Section 3.1, even in nonintegrable systems it is possible to derive a logarithmic bound for the growth of the Rényi OSE entropies for operators that are linked with a conserved quantity [38] and exhibit a power-law decaying ITAC. To investigate operators spreading in the presence of integrability-breaking perturbations, in Fig. 9 we plot $S_n(S^z)$ for the deformed XXZ chain (cf. (9)) with $\Delta = 3$ and $\Delta' = 1/4\Delta$. For nonzero Δ' the Hamiltonian in Eq. (9) is nonintegrable. In particular, by using standard diagnostic tools for chaotic systems, such as the distribution of energy levels, one can check that the spectrum of (9) is compatible with that of a chaotic Hamiltonian. In Fig. 9 we show the von Neumann entropy for several values of the bond dimension $\chi = 50, 100, 200, 400, 800, 1600, 2500$ (continuous lines from bottom to top). As already discussed in Ref. [15], it is challenging to obtain the asymptotic behavior of S_1 at $t \rightarrow \infty$. Precisely, the data at $t \lesssim 10$ suggest a linear increase (see dashed-dotted line in the Figure). However, it is not clear whether the bending of the curves at long times signals a change in the behavior of S_1 , or it is due to truncation of the bond dimension. In Fig. 9 we also show results for S_n with $n = 2, 3, 4, \infty$. Now, the growth of S_n is much weaker. We observe that the convergence with increasing χ is faster. This is expected because the Rényi entropies are more sensitive to the lower part of the ES , which is better captured even at small χ . Indeed, in Fig. 9 the data for S_n with $n > 2$ are obtained with $\chi = 1600$. Now, in contrast with S_1 , S_n are compatible with a logarithmic increase for $n > 1$. Indeed, since the global magnetization is preserved by (9), even for nonzero Δ' ,

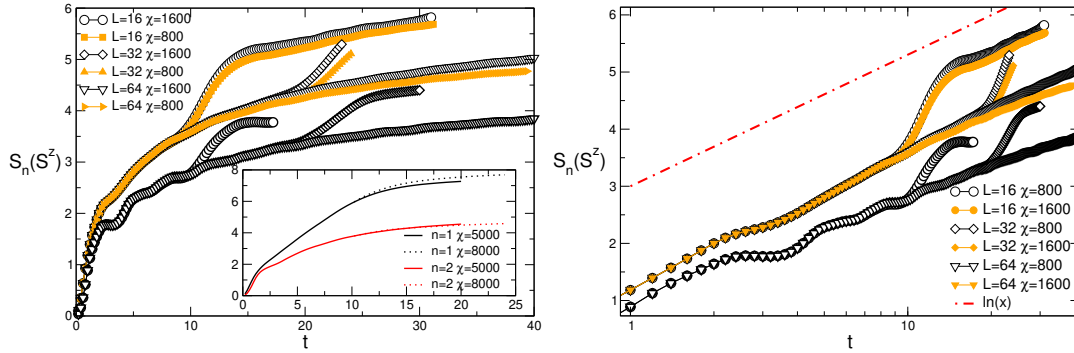


Figure 10. Revival effects in the dynamics of the operator entanglement S_n for S^z . Both panels show $tDMRG$ data for the XXZ chain with $\Delta = 3$. Left panel: dynamics of S_n for a chain with $L = 16, 32, 64$ (different symbols) and two values of the bond dimension $\chi = 800, 1600$. We show results for $n = 1$ and $n = 2$. Revivals at $t \approx L/2$ are visible. The inset shows the effect of integrability breaking. The curves are $tDMRG$ data for the XXZ chain with $\Delta = 3$ and $\Delta' = 0.25\Delta$. The data are for $L = 16$ and $n = 1, 2$ with $\chi = 5000, 8000$. The data show no revivals. Right panel: Same data as in the main left panel using the logarithmic scale on the x -axis. The dash-dotted line is $\ln(t)$.

it is reasonable to expect a power-law decaying $ITACC$. In turn, this implies (cf. (10)) at most logarithmic growth of the OSE entropies of S^z . This is also confirmed in the right panel of Fig. 9 where we employ a logarithmic scale on the x axis. Notice that the prefactor of the putative logarithmic growth is $\sim 1/2 \ln(t)$, i.e., even smaller than in the integrable case (see Fig. 8). Indeed, based on the behavior in Fig. 9, one cannot exclude that S_n saturate at long times.

5.3. Entanglement “revivals” & integrability breaking

It is interesting to investigate the effect of the finite-size of the chain in the dynamics of the operator entropies. It has been shown in Ref. [49] that in finite-size integrable chains the dynamics of the state entanglement after a global quantum quench exhibits “revivals”. The origin of revivals is that in integrable systems information spreads via the ballistic transport of quasiparticles. Moreover, quantum correlations between pairs of quasiparticles are preserved during their dynamics [1, 2, 5]. The entanglement between two spatial regions is due to entangled pairs that are shared between the regions. Now, if the regions are embedded in a *finite* chain the motion of the quasiparticles is periodic, implying periodicity in the contribution of the pairs to the entanglement between the regions. This explains revivals in the entanglement of a state. Notice that since not all the entangled pairs travel at the same velocity, the entanglement revivals weaken with the revival time [49]. This is a weak form of quantum information scrambling [50] for integrable systems. Oppositely, it was shown in Ref. [49] that for dynamics under nonintegrable Hamiltonians, revivals are more strongly suppressed. The reason is that entanglement dynamics in nonintegrable systems does not happen via quasiparticle

spreading. Instead, information is quickly dispersed in the global degrees of freedom by the dynamics.

Here we show that revivals occur in the operator entanglement spreading in finite chains, although they have a different origin. In the following we focus on the dynamics of traceless operators in the deformed *XXZ* chain (9). Our *tDMRG* are reported in Fig. 10. In the left panel of Fig. 10 we plot $S_n(S^z)$ for the *XXZ* chain with $\Delta = 3$ ($\Delta' = 0$ in (9)). We focus on $n = 1$ and $n = 2$. We plot with different symbols (circles, diamonds, and triangles) the dynamics in chains of different sizes $L = 16, 32, 64$. For $n = 1$ the empty symbols correspond to $\chi = 1600$, whereas the full symbols are the results for $\chi = 800$. For $n = 2$ we only show the results for $\chi = 1600$, because it is sufficient to ensure convergence. We plot the same data in the right panel in Fig. 10 using a logarithmic scale on the x axis. The revivals of the entropies are clearly visible. Interestingly, the prefactor of the logarithmic growth after the revival remains the same. Notice that the velocity of the quasiparticles, and hence the time of the revivals, could be determined via the Thermodynamic Bethe Ansatz approach [19]. Let us now discuss the mechanism underlying these revivals. First, as it is clear from the case of the rule 54 chain, (see Section 2.1), the growth of the entropies is not due to the propagation of entangled pairs. Instead, the growth of the *OSE* is due to the fact that the information needed to detect the position of the solitons generated by the operator insertion at the center grows with time. Now, the “kicks” at the revivals can be interpreted as the extra information needed to decide whether the solitons emitted at the center were reflected at the boundaries or not. Let us now discuss the effect of breaking integrability. We show *tDMRG* data for the nonintegrable *XXZ* chain with $L = 16$ with $\Delta = 3$ and $\Delta' = \Delta/4$ in the inset of Fig. 10. The data do not show any sign of entanglement revivals. This is consistent with the fact that in nonintegrable systems information is not spread by propagation of quasiparticles.

6. Conclusions

We numerically investigated the dynamics of the Rényi Operator Space Entanglement (*OSE*) entropies in one dimensional systems. We focused on both integrable and nonintegrable systems. We first discussed the paradigmatic case of the rule 54 chain. We showed that the Rényi operator entanglement entropies S_n of traceless operators grow logarithmically with time for any n . The prefactor of the logarithmic growth depends on n in a nontrivial manner. On the other hand, for operators that have nonzero trace, S_n grow logarithmically only for $n = 1$. For $n > 1$, S_n saturate in the limit $t \rightarrow \infty$, and the saturation values are determined by the operator trace. Moreover, our results suggest that the full entanglement spectrum of operators with nonzero trace can be reconstructed from the entanglement spectrum of their traceless part. Interestingly, the scenario is similar for the *XXZ* chain, which is a prototypical Bethe ansatz integrable model. Specifically, the entropies of operators with nonzero trace grow logarithmically for $n = 1$, whereas they saturate for $n > 1$. For traceless operators, S_n grows logarithmically for any

n . The prefactors of the logarithmic growth are compatible with the ones numerically obtained for the rule 54 chain.

We next discussed operator spreading in nonintegrable dynamics. As it was shown in Ref. [15], it is challenging to extract the asymptotic behavior of S_1 at long times. On the other hand, the growth of S_n for $n > 1$ is milder as compared with $n = 1$, and it is compatible with a logarithmic growth, at least for the models that we considered. Finally, we showed that in finite integrable systems, S_n exhibit revivals. After the revivals S_n continue growing logarithmically with time. Interestingly, upon switching on integrability-breaking interactions, revivals disappear, signaling the absence of well-defined quasiparticles.

There are several directions for future research. First, it is important to clarify the scaling of the *OSE* entropies in nonintegrable systems. This is a challenging task, as already pointed out in Ref. [15], because of strong finite-time corrections. Furthermore, it would be important to clarify the mechanism underlying the growth of *OSE* in integrable systems. Precisely, the fact that the prefactor of the logarithmic growth of the entropies is the same for both the rule 54 chain and the *XXZ* chain suggests that it could be universal. It would be useful to numerically extract the prefactor of the logarithmic growth by using the *MPO* representation of local operators [24, 14, 51] in the rule 54 chain. This will allow to clarify the relationship between *OSE* growth and transport properties. Notice that a deep relationship between operator growth and transport has been already established in Ref. [52] for some one-dimensional systems subject to dephasing. Moreover, it would be interesting to investigate the *OSE* growth in random unitary circuits with $U(1)$ conservation laws, by employing the results of Refs. [53, 54]. On the analytical side, one could try to explore the relationship [55] between *OSE* and Out-of-Time-Order-Correlators (*OTOC*). Finally, having access to the asymptotic behavior of the Rényi entropies would allow to reconstruct the structure of the operator entanglement spectrum.

Acknowledgements

This paper is dedicated to the memory of Marko Medenjak who left us before his time. In his brief journey Marko has left many important contributions that helped shape my interest in operator spreading. More importantly, our discussions stimulated many interesting questions, some of which are explored in this work.

This study was carried out within the National Centre on HPC, Big Data and Quantum Computing - SPOKE 10 (Quantum Computing) and received funding from the European Union Next-GenerationEU - National Recovery and Resilience Plan (NRRP) – MISSION 4 COMPONENT 2, INVESTMENT N. 1.4 – CUP N. I53C22000690001. This work has been supported by the project “Artificially devised many-body quantum dynamics in low dimensions - ManyQLowD” funded by the MIUR Progetti di Ricerca di Rilevante Interesse Nazionale (PRIN) Bando 2022 - grant 2022R35ZBF.

References

- [1] Calabrese P and Cardy J 2005 *Journal of Statistical Mechanics: Theory and Experiment* **2005** P04010 URL <https://doi.org/10.1088/1742-5468/2005/2F04/2Fp04010>
- [2] Fagotti M and Calabrese P 2008 *Phys. Rev. A* **78**(1) 010306 URL <https://link.aps.org/doi/10.1103/PhysRevA.78.010306>
- [3] Kim H and Huse D A 2013 *Phys. Rev. Lett.* **111**(12) 127205 URL <https://link.aps.org/doi/10.1103/PhysRevLett.111.127205>
- [4] Liu H and Suh S J 2014 *Phys. Rev. Lett.* **112**(1) 011601 URL <https://link.aps.org/doi/10.1103/PhysRevLett.112.011601>
- [5] Alba V and Calabrese P 2017 *Proceedings of the National Academy of Sciences* **114** 7947–7951 ISSN 0027-8424 (Preprint <https://www.pnas.org/content/114/30/7947.full.pdf>) URL <https://www.pnas.org/content/114/30/7947>
- [6] Bertini B, Klobas K, Alba V, Lagnese G and Calabrese P 2022 *Phys. Rev. X* **12**(3) 031016 URL <https://link.aps.org/doi/10.1103/PhysRevX.12.031016>
- [7] Schollwöck U 2011 *Annals of Physics* **326** 96–192 ISSN 0003-4916 january 2011 Special Issue URL <https://www.sciencedirect.com/science/article/pii/S0003491610001752>
- [8] Paeckel S, Köhler T, Swoboda A, Manmana S R, Schollwöck U and Hubig C 2019 *Annals of Physics* **411** 167998 ISSN 0003-4916 URL <https://www.sciencedirect.com/science/article/pii/S0003491619302532>
- [9] Prosen T and Žnidarič M 2007 *Phys. Rev. E* **75**(1) 015202 URL <https://link.aps.org/doi/10.1103/PhysRevE.75.015202>
- [10] Zanardi P 2001 *Phys. Rev. A* **63**(4) 040304 URL <https://link.aps.org/doi/10.1103/PhysRevA.63.040304>
- [11] Prosen T and Pižorn I 2007 *Phys. Rev. A* **76**(3) 032316 URL <https://link.aps.org/doi/10.1103/PhysRevA.76.032316>
- [12] Pižorn I and Prosen T 2009 *Phys. Rev. B* **79**(18) 184416 URL <https://link.aps.org/doi/10.1103/PhysRevB.79.184416>
- [13] Dubail J 2017 *Journal of Physics A: Mathematical and Theoretical* **50** 234001 URL <https://dx.doi.org/10.1088/1751-8121/aa6f38>
- [14] Alba V, Dubail J and Medenjak M 2019 *Phys. Rev. Lett.* **122**(25) 250603 URL <https://link.aps.org/doi/10.1103/PhysRevLett.122.250603>
- [15] Alba V 2021 *Phys. Rev. B* **104**(9) 094410 URL <https://link.aps.org/doi/10.1103/PhysRevB.104.094410>
- [16] Bobenko Alexander and Bordemann M, Gunn C and Pinkall U 1993 *Communications in Mathematical Physics* **158** 127–134 ISSN 1432-0916 URL <https://doi.org/10.1007/BF02097234>
- [17] Buča B, Klobas K and Prosen T 2021 *Journal of Statistical Mechanics: Theory and Experiment* **2021** 074001 URL <https://dx.doi.org/10.1088/1742-5468/ac096b>
- [18] Gopalakrishnan S 2018 *Phys. Rev. B* **98**(6) 060302 URL <https://link.aps.org/doi/10.1103/PhysRevB.98.060302>
- [19] Gopalakrishnan S, Huse D A, Khemani V and Vasseur R 2018 *Phys. Rev. B* **98**(22) 220303 URL <https://link.aps.org/doi/10.1103/PhysRevB.98.220303>
- [20] Prosen T and Mejía-Monasterio C 2016 *Journal of Physics A: Mathematical and Theoretical* **49** 185003 URL <https://dx.doi.org/10.1088/1751-8113/49/18/185003>
- [21] Gopalakrishnan S and Zakirov B 2018 *Quantum Science and Technology* **3** 044004 URL <https://dx.doi.org/10.1088/2058-9565/aad759>
- [22] Buča B, Garrahan J P, Prosen T and Vanicat M 2019 *Phys. Rev. E* **100**(2) 020103 URL <https://link.aps.org/doi/10.1103/PhysRevE.100.020103>
- [23] Rowlands D A and Lamacraft A 2018 *Phys. Rev. B* **98**(19) 195125 URL <https://link.aps.org/doi/10.1103/PhysRevB.98.195125>

- [24] Klobas K, Medenjak M, Prosen T and Vanicat M 2019 *Communications in Mathematical Physics* **371** 651–688 ISSN 1432-0916 URL <https://doi.org/10.1007/s00220-019-03494-5>
- [25] Nahum A, Ruhman J, Vijay S and Haah J 2017 *Phys. Rev. X* **7**(3) 031016 URL <https://link.aps.org/doi/10.1103/PhysRevX.7.031016>
- [26] Jonay C, Huse D A and Nahum A 2018 Coarse-grained dynamics of operator and state entanglement (*Preprint* 1803.00089) URL <https://arxiv.org/abs/1803.00089>
- [27] Chan A, De Luca A and Chalker J T 2018 *Phys. Rev. X* **8**(4) 041019 URL <https://link.aps.org/doi/10.1103/PhysRevX.8.041019>
- [28] von Keyserlingk C W, Rakovszky T, Pollmann F and Sondhi S L 2018 *Phys. Rev. X* **8**(2) 021013 URL <https://link.aps.org/doi/10.1103/PhysRevX.8.021013>
- [29] Zhou T and Nahum A 2020 *Phys. Rev. X* **10**(3) 031066 URL <https://link.aps.org/doi/10.1103/PhysRevX.10.031066>
- [30] Bertini B and Piroli L 2020 *Phys. Rev. B* **102**(6) 064305 URL <https://link.aps.org/doi/10.1103/PhysRevB.102.064305>
- [31] Bertini B, Kos P and Prosen T 2020 *SciPost Phys.* **8** 067 URL <https://scipost.org/10.21468/SciPostPhys.8.4.067>
- [32] Bertini B, Kos P and Prosen T 2020 *SciPost Phys.* **8** 068 URL <https://scipost.org/10.21468/SciPostPhys.8.4.068>
- [33] Claeys P W and Lamacraft A 2020 *Phys. Rev. Res.* **2**(3) 033032 URL <https://link.aps.org/doi/10.1103/PhysRevResearch.2.033032>
- [34] Foligno A, Zhou T and Bertini B 2023 *Phys. Rev. X* **13**(4) 041008 URL <https://link.aps.org/doi/10.1103/PhysRevX.13.041008>
- [35] Rampp M A, Moessner R and Claeys P W 2023 *Phys. Rev. Lett.* **130**(13) 130402 URL <https://link.aps.org/doi/10.1103/PhysRevLett.130.130402>
- [36] Rampp M A, Rather S A and Claeys P W 2024 *Phys. Rev. Res.* **6**(3) 033271 URL <https://link.aps.org/doi/10.1103/PhysRevResearch.6.033271>
- [37] Lopez-Piqueres J, Ware B, Gopalakrishnan S and Vasseur R 2021 *Phys. Rev. B* **104**(10) 104307 URL <https://link.aps.org/doi/10.1103/PhysRevB.104.104307>
- [38] Muth D, Unanyan R G and Fleischhauer M 2011 *Phys. Rev. Lett.* **106**(7) 077202 URL <https://link.aps.org/doi/10.1103/PhysRevLett.106.077202>
- [39] Calabrese P and Lefevre A 2008 *Phys. Rev. A* **78**(3) 032329 URL <https://link.aps.org/doi/10.1103/PhysRevA.78.032329>
- [40] Wigner E P 1955 *Phys. Rev.* **98**(1) 145–147 URL <https://link.aps.org/doi/10.1103/PhysRev.98.145>
- [41] Takahashi M 1999 *Thermodynamics of One-Dimensional Solvable Models* (Cambridge University Press)
- [42] Alba V and Calabrese P 2018 *SciPost Phys.* **4**(3) 17 URL <https://scipost.org/10.21468/SciPostPhys.4.3.017>
- [43] Bertini B, Collura M, De Nardis J and Fagotti M 2016 *Phys. Rev. Lett.* **117**(20) 207201 URL <https://link.aps.org/doi/10.1103/PhysRevLett.117.207201>
- [44] Castro-Alvaredo O A, Doyon B and Yoshimura T 2016 *Phys. Rev. X* **6**(4) 041065 URL <https://link.aps.org/doi/10.1103/PhysRevX.6.041065>
- [45] Mirsky L 1975 *Monatshefte für Mathematik* **79** 303–306 ISSN 1436-5081 URL <https://doi.org/10.1007/BF01647331>
- [46] Doyon B 2020 *SciPost Phys. Lect. Notes* 18 URL <https://scipost.org/10.21468/SciPostPhysLectNotes.18>
- [47] Vecchio G D V D and Doyon B 2022 *Journal of Statistical Mechanics: Theory and Experiment* **2022** 053102 URL <https://dx.doi.org/10.1088/1742-5468/ac6667>
- [48] Medenjak M 2022 *Journal of Physics A: Mathematical and Theoretical* **55** 404002 URL <https://dx.doi.org/10.1088/1751-8121/ac8fc4>
- [49] Modak R, Alba V and Calabrese P 2020 *Journal of Statistical Mechanics: Theory and Experiment*

- 2020** 083110 URL <https://dx.doi.org/10.1088/1742-5468/aba9d9>
- [50] Alba V and Calabrese P 2019 *EPL (Europhysics Letters)* **126** 60001 URL <https://doi.org/10.1209/0295-5075/126/60001>
- [51] Foligno A and Bertini B 2024 (*Preprint* [2408.16750](https://arxiv.org/abs/2408.16750)) URL <https://arxiv.org/abs/2408.16750>
- [52] Wellnitz D, Preisser G, Alba V, Dubail J and Schachenmayer J 2022 *Phys. Rev. Lett.* **129**(17) 170401 URL <https://link.aps.org/doi/10.1103/PhysRevLett.129.170401>
- [53] Rakovszky T, Pollmann F and von Keyserlingk C W 2019 *Phys. Rev. Lett.* **122**(25) 250602 URL <https://link.aps.org/doi/10.1103/PhysRevLett.122.250602>
- [54] Huang Y 2020 *IOP SciNotes* **1** 035205 URL <https://dx.doi.org/10.1088/2633-1357/abd1e2>
- [55] Dowling N, Kos P and Modi K 2023 *Phys. Rev. Lett.* **131**(18) 180403 URL <https://link.aps.org/doi/10.1103/PhysRevLett.131.180403>